NJC

ROYAL SOCIETY OF CHEMISTRY

PAPER

View Article Online
View Journal | View Issue

Cite this: *New J. Chem.*, 2025, **49**, 18716

Structural and photophysical features of triphenylene–gold(I) phosphane complexes†

Anyie P. Atencio,[a] Alba Sevillano,[a] Ariadna Lázaro,[ab] Zoraida Freixa,[cd] David Aguilà,[ab] Inmaculada Angurell[ab] and Laura Rodríguez *[ab]

Two series of mono- or dinuclear gold(I) complexes incorporating an ethynyltriphenylene chromophore and various mono- and diphosphanes have been synthesized and characterized to explore the interplay between the ligand structure, aurophilic interactions, and photophysical properties. The complexes display dual emission behaviour, with fluorescence dominating under air-equilibrated conditions and phosphorescence emerging under oxygen-free environments. Dinuclear compounds bearing diphosphane linkers show enhanced phosphorescence, attributed to shorter Au(I)···Au(I) distances that facilitate intersystem crossing (ISC). Upon immobilization in PMMA matrices, all selected compounds exhibit efficient room-temperature phosphorescence even in the presence of oxygen, with emission quantum yields up to 33% and lifetimes extending to nearly one millisecond. These findings highlight the potential of structural design and matrix confinement to engineer metal-based luminophores for applications in time-gated imaging, security inks, and light-emitting devices.

Received 22nd August 2025,
Accepted 23rd September 2025

DOI: 10.1039/d5nj03389f

rsc.li/njc

Introduction

Heavy metal-based luminescent systems have drawn a great deal of interest because of their wide application in fields such as OLEDs, sensing, security inks, anticancer agents and bioimaging.[1–9] In particular, gold(I) complexes present peculiar photophysical properties and the ability to undergo aurophilic interactions.[10,11] The presence of a heavy atom, as well as aggregation through several types of weak interactions, is often exploited in tuning phosphorescence since intersystem crossing (ISC) is regularly facilitated.[12–16] This is due to the relativistic effects that lead to a strong contraction of the s and p orbitals, particularly the outermost 6s orbital. In contrast, the inner 5d orbitals are shielded by the contracted s and p electrons, leading to a compensatory expansion and an increase in their energy. In this context, gold(I) complexes are of interest since phosphorescence is known to occur at accessible temperatures with many of them, and aurophilicity has been employed in the design of supramolecularly aggregated systems.[17–25]

At the same time, playing with nuclearity (mono- *vs.* dinuclear), flexibility/rigidity and conformation of the bridging ligands is key for the resulting photophysical properties. These factors will ultimately govern the resulting supramolecular assemblies generated, including the establishment of both intra- and intermolecular contacts, and the emissions present as a result (fluorescence, phosphorescence or dual emission).[26–32]

The insertion of a gold(I) centre into a π-conjugated backbone (alkynylated aromatics) can represent a solid foundation on which to build emissive structures, with a tuneable electronic structure and molecular arrangement.[3,6,10,33] Triphenylene, a fully planar, rigid polycyclic aromatic hydrocarbon, is an interesting and easily accessible skeleton to be used as a luminophore, and its ethynyl-functionalization makes it capable of being coordinated directly to gold(I) through a conjugated system.

Additionally, phosphine ligands, and in particular mono and diphosphines, provide further modularity through their electronic properties, steric demand and conformational flexibility. A variety of mono- and dinuclear gold(I) complexes were synthesized, structurally characterized, and their photophysical properties were investigated.[6,10,11,14,15,18,31–34] The aim of this study is to determine if and how the nature of the phosphine (basicity, bulkiness, and rigidity) tunes the emission properties of these complexes. Moreover, the effect of immobilization in a PMMA matrix was also investigated, as a means to quench non-radiative decay channels and access room-temperature phosphorescence.

[a] *Departament de Química Inorgànica i Orgànica, Secció de Química Inorgànica, Universitat de Barcelona, Martí i Franquès 1-11, E-08028 Barcelona, Spain. E-mail: laurarodriguezr@ub.edu*
[b] *Institut de Nanociència i Nanotecnologia (IN²UB), Universitat de Barcelona, 08028 Barcelona, Spain*
[c] *Facultad de Química, Universidad del País Vasco (UPV/EHU), San Sebastián, 20018, Spain*
[d] *IKERBASQUE, Basque Fundation for Science, Bilbao, 48013, Spain*

† Dedicated to Professor Resnati, celebrating a career in fluorine and noncovalent chemistry on the occasion of his 70th birthday.

Results and discussion

Synthesis and characterization

Two series of gold(I) complexes, five mononuclear (series 1) and four dinuclear (series 2), have been synthesized following a general procedure outlined in Scheme 1. All compounds feature the same 2-ethynyltriphenylene ligand (**L**) as the chromophore and differ in the solubility, rigidity, and steric hindrance of their phosphane units.

The complexes were successfully characterized by ^{1}H and ^{31}P{^{1}H} NMR, and IR spectroscopy and mass spectrometry. The ^{31}P{^{1}H} NMR spectra display, in all cases, a sharp singlet approximately 50–60 ppm downfield-shifted relative to the free phosphine, which is consistent with that previously reported for similar complexes.[13–15,18,20] The presence of only one singlet also in the case of derivatives **2** confirms the binuclear structure of these compounds and the equivalence of their phosphorus atoms in solution. In the ^{1}H NMR spectra, the signals corresponding to both the chromophore and the phosphine moieties were clearly observed with the expected integration and were perfectly assigned thanks to ^{13}C and HSQC NMR spectra. These spectra also reflect the symmetry of the diphosphine ligands within the complex in solution. Additionally, ESI(+) mass spectrometry confirmed the formation of the desired complexes through the detection of the corresponding $[M + H]^+$ or $[M + Na]^+$ molecular ions.

Crystals suitable for single crystal X-ray diffraction were obtained by slow diffusion of Et_2O or hexane, respectively, into dichloromethane solutions of **1c** or **2i**. The compounds crystallize in the $P\bar{1}$ (**1c**) and $P2_1/c$ (**2i**) space groups of the triclinic and monoclinic crystal systems, respectively, and confirm the structure and nuclearity of each series. The corresponding molecular structures are presented in Fig. 1 and selected bond lengths and angles are summarized in Table 1.

Compound **1c** exhibits two mononuclear molecules in the asymmetric unit, each of them showing the bonding between the PPh_3 phosphine and the gold precursor. A near linear geometry around the gold atom is observed, with P–Au–C angles of 176.9(2) and 172.7(2)°, respectively. Compound **2i** demonstrates the dinuclear nature of series 2, with the diphosphine connecting the two Au**L** units and promoting a short intermolecular Au(I)···Au(I) interaction between both gold cations (3.0998(5) Å). The values of the corresponding P–Au–C angles (172.8(2) and 175.4(2)°) are similar to **1c**, showing again a slight departure from a linear arrangement. For both compounds, the Au–C and C≡C distances and P–Au–C and

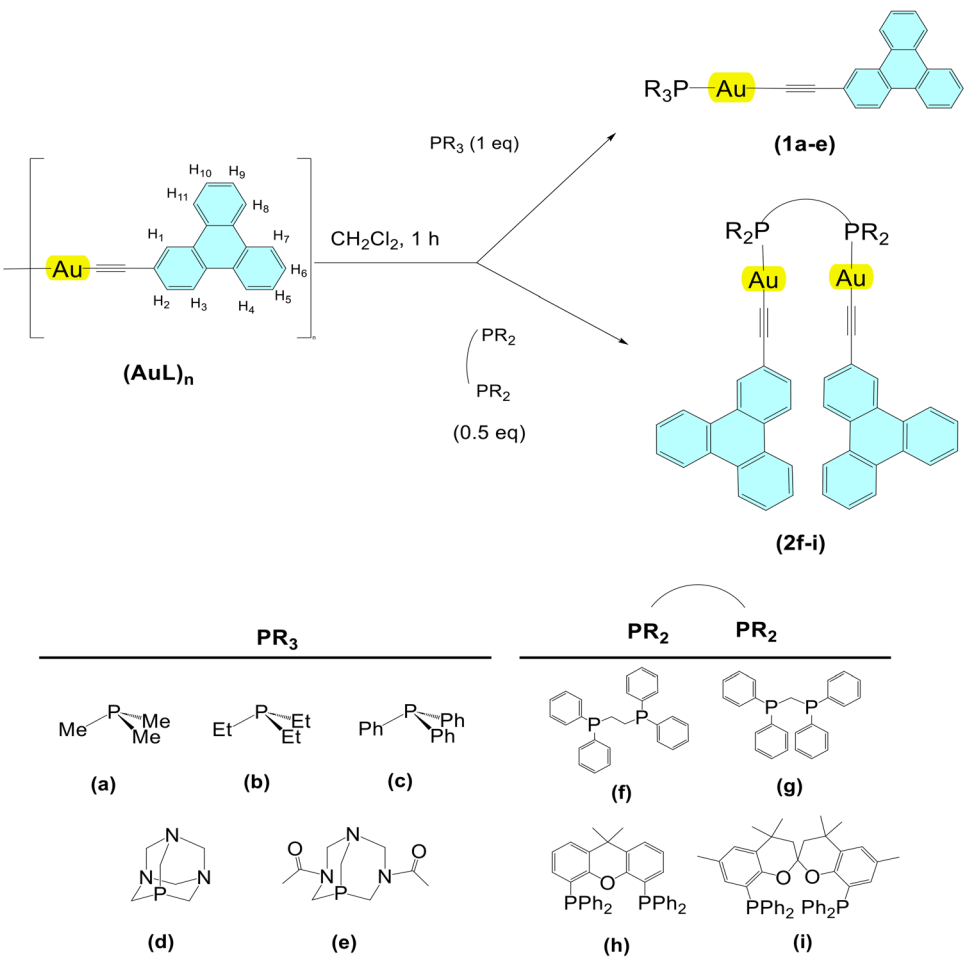

Scheme 1 Synthesis of gold(I) phosphane complexes.

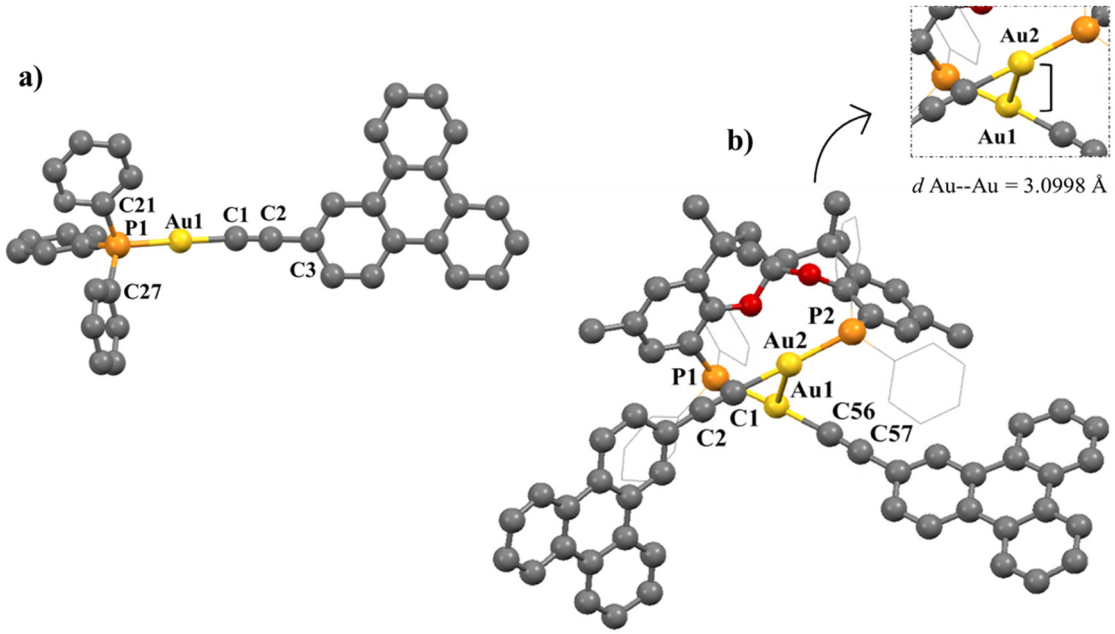

Fig. 1 X-ray crystal structures of **1c** (a) and **2i** (c). Solvates and hydrogen atoms were omitted for clarity. Colour key: yellow = Au; orange = P; grey = C.

Au–C≡C angles (Table 1) are in the usual ranges for Au(I) alkynyl complexes.[10,34]

The 3D packing of the mononuclear complexes exhibits a conformation driven by the establishment of π–π and C–H···π interactions. In complex **1c**, the intermolecular interactions occur in two ways: (1) between the alkyl/aryl substituents of the phosphine and the triphenylene unit, and (2) between the C–H groups of the triphenylene and the C≡C group of a neighbouring molecule, as shown in Fig. S44. As a result, the molecules arrange themselves into alternating dimers relative to each other, although they are not entirely parallel. In the case of the bimetallic complex **2i**, the molecular structure reflects the spiral structure of the chiral ligand. As the ligand has been used as a racemate, the compound crystallizes in a centrosymmetric group containing both enantiomers. The unit cell could be described as containing the centroid of four molecules (two pairs of enantiomers), in addition to 4 solvent molecules. Each pair of enantiomers is related by a glide plane and both pairs relate one each other through an inversion centre located in the middle point of the unit cell (see Fig. S44). The ligand used, SPANphos, is a highly flexible ligand originally designed as a *trans*-chelator.[35] In **2i** the spirobichromane backbone of the ligand adopts an extended conformation with the spiro rings in what has been described as a boat–boat conformation, similar to that encountered in other dinuclear SPANphos complexes.[36] Accordingly, in this conformation, the two phosphorus atoms are at a rather large distance, and coordinate to two different gold(I) centres, in a bridging manner (5.791(3) Å). Eventually, the final conformation is stabilized by the intramolecular Au(I)···Au(I) interaction, forcing the disposition of the two triphenylene moieties in a cross-like spatial arrangement. No intermolecular aurophilic interactions are present in **2i**.

Table 1 Selected bond lengths (Å) and angles (deg) for complexes

Distance	[Å]	Angle	[°]
1c			
Au(1)–C(1)	2.005(6)	P(1)–Au(1)–C(1)	176.9(2)
Au(2)–C(39)	2.016(8)	P(2)–Au(2)–C(51)	172.7(2)
P(1)–Au(1)	2.2737(18)	Au(1)–P(1)–C(21)	113.6(2)
P(2)–Au(2)	2.278(2)	Au(2)–P(2)–C(71)	117.5(3)
P(1)–C(21)	1.802(7)	C(1)–C(2)–C(3)	175.5(8)
P(2)–C(71)	1.829(8)	C(39)–C(40)–C(41)	176.5(9)
C(1)–C(2)	1.189(9)		
C(39)–C(40)	1.183(11)		
2i			
Au(1)–Au(2)	3.0998(5)	P1–Au1–C56	172.8(2)
P1–Au1	2.284(2)	P2–Au2–C1	175.4(2)
Au1–C56	2.031(9)	C1–C2–C3	178.4(9)
Au2–P2	2.287(2)	C58–C57–C56	174.8(9)
Au2–C1	2.023(9)	Au1–Au2–P2	103.58(6)
C1–C2	1.19(1)	Au2–Au1–P1	107.93(6)
C57–C56	1.16(1)	Au2–C1–C2	178.2(8)
		Au1–C56–C57	174.7(8)

Photophysical characterization

Absorption and emission spectra were recorded in 4.0×10^{-6} M dichloromethane solutions for all complexes and the organic precursor ligand **L** with the results summarized in Table 2. Dichloromethane was selected as the ideal solvent due to the apolar nature of the complexes, which limited their solubility in more polar or biocompatible solvents.

The absorption spectra of all the compounds display characteristic bands between 250 and 350 nm, attributed to π–π* intraligand transitions associated with the triphenylene ligand (Fig. 2). These bands are *ca.* 10–20 nm red-shifted for the gold(I) complexes with respect to **L**. The lowest-energy absorption bands are attributed to π → π* charge transfer

Table 2 Absorption and emission data of the different series of compounds in dichloromethane at 4.0×10^{-6} M and ratio of phosphorescence and fluorescence intensities, I_P/I_F, in N_2-sat solutions

Compound	Absorption λ_{max}, nm ($\varepsilon \times 10^4$ M^{-1} cm^{-1})	Fluorescence emission air-eq., λ_{max} (nm)	Phosphorescence emission N_2-sat, λ_{max} (nm)	I_{Ph}/I_{Fl}
L	268 (9.79), 290 (1.17)	375	—	—
1a	278 (8.44), 310 (3.50), 324 (4.52)	380	520	0.44
1b	278 (5.82), 310 (2.73), 324 (3.51)	380	520	2.67
1c	279 (4.83), 309 (2.46), 328 (3.39)	379	520	3.87
1d	278 (5.72), 310 (3.10), 328 (4.06)	367	520	8.02
1e	277 (6.46), 310 (4.43), 327 (4.42)	380	520	11.72
2f	277 (10.7), 310 (5.58), 327 (7.36)	380	520	0.95
2g	279 (8.03), 315 (4.08), 331 (3.70)	382	522	8.78
2h	277 (3.64), 315 (1.66), 332 (1.73)	382	524	4.52
2i	278 (12.4), 315 (6.18), 329 (7.42)	382	524	5.19

nature transitions while the following prominent band is assigned to a combined character of intra-ligand charge transfer (ILCT) and ligand-to-metal charge transfer (LMCT), in agreement with previous theoretical calculations.[31] Lower absorption intensities and broad bands were recorded for dppm (**2g**) and xantphos (**2h**) derivatives due to lower solubility and formation of small aggregates under these conditions.

The emission spectra of the gold(I) complexes show a vibronically structured fluorescence band as the dominant emission under air-equilibrated conditions, while phosphorescence becomes the most intense emissive band upon oxygen removal (N_2-saturated samples, Fig. 3). The emergence of phosphorescence is attributed to the heavy atom effect of the Au(I) centre, as evidenced by the purely fluorescence emission observed for the organic precursor ligand. Among the mononuclear complexes, compounds **1d** and **1e** (featuring PTA and DAPTA ligands, respectively) exhibited lower solubility in organic solvents and displayed a greater contribution from phosphorescence.[37] Analysis of the emission spectra of the dinuclear complexes reveals an increased phosphorescence-to-fluorescence intensity ratio for compounds **2g**, **2h**, and **2i** (see Table 2). Notably, compound **2g** shows significant band broadening (also detected in the NMR spectrum, see the SI), which, along with the reduced solubility observed in its absorption spectrum, suggests close proximity between the gold(I) centres, as in the case of **2i**.[28] This spatial arrangement, likely maintained in solution due to the structural disposition of the two Au(I) atoms, facilitates intersystem crossing and enhances the phosphorescence emission. As expected, these aurophilic interactions are less important for **2f**, that contains the more flexible dppe diphosphane as the bridging ligand. The effect of the gold(I) atom in the intersystem crossing is also reflected in the resulting fluorescence and phosphorescence quantum yields (see Table 3) that are one order of magnitude smaller for the gold(I) complexes with respect to **L**.

Emission lifetimes of the fluorescence bands are in the order of 10 ns, supporting the fluorescence assignment as ^{1}IL emission (see Table 3).[31,38,39] The vibronically structured shape of the red-shifted emission and comparison with the literature,[14,30,31] together with the recorded emission lifetimes in the order of microseconds, supports an ^{3}IL assignment. Phosphorescence emission lifetimes are around 100–145 μs for the mononuclear compounds while they are smaller for the dinuclear ones. Compounds **2f** and **2i** are those with the larger phosphorescence quantum yields and lifetimes within the dinuclear series, probably due to the lower possibility of intramolecular aurophilic contacts for the compounds containing the more flexible conformations. The smaller phosphorescence efficiency of the dinuclear compounds (φ°_{Ph}) with respect

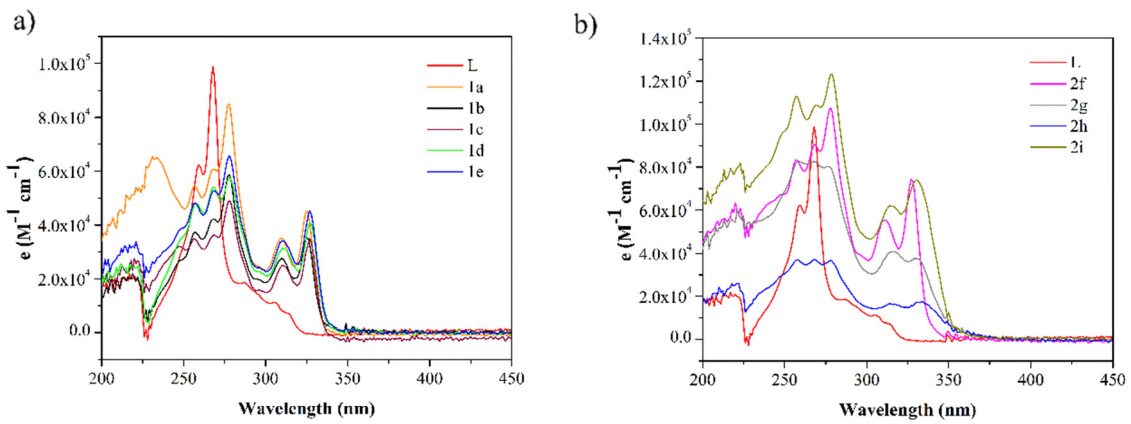

Fig. 2 Absorption spectra of 4.0×10^{-6} M dichloromethane solutions of (a) series 1 and (b) series 2 complexes.

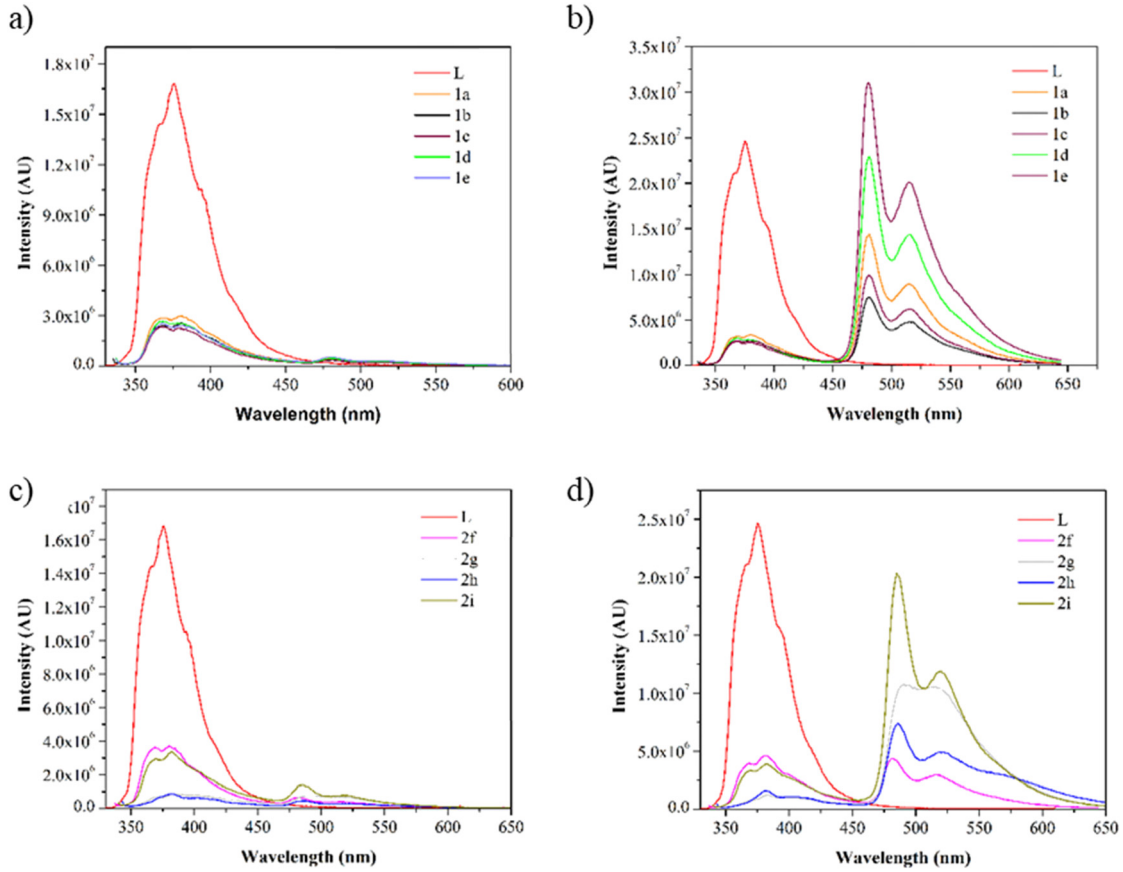

Fig. 3 Emission spectra of monophosphane series (a) and diphosphane series (c) under air-equilibrated conditions (left) and N_2-saturated conditions (b and d, right) of 4.0 × 10^{-6} M dichloromethane solutions, λ_{exc} = 310 nm.

Table 3 Luminescence quantum yields and lifetimes recorded for all the compounds in dichloromethane

Compound	ϕ_{Fl} (air-eq.)	φ°_{Ph} (N_2 sat.)	τ_{Fl} (ns) (air-eq.)	τ°_{Ph} (μs) (N_2 sat.)
L	0.04	—	9.1	—
1a	<1%	0.09	10.9	134
1b	<1%	0.07	9.2	85
1c	<1%	0.06	9.9	96
1d	<1%	0.09	8.9	144
1e	<1%	0.10	8.8	100
2f	<1%	0.04	8.9	5
2g	<1%	0.02	9.5	60
2h	<1%	0.03	8.3	18
2i	<1%	0.05	10.0	13

to the mononuclear ones can be ascribed to more favoured deactivation processes, in agreement with the larger values of k_{nr}, that are expected to be more favoured in the presence of intramolecular aurophilic contacts (see Table S3).

Immobilization of the compounds in PMMA matrixes

To reduce non-radiative deactivation processes, we investigated how the emission properties change when the compounds are immobilized in solid matrices, selecting PMMA as the host material for this purpose.[40,41] Two complexes from each series were selected for this purpose, based on differences in the size and flexibility of the (di)phosphine ligands, with **1a** and **1e** from series 1 and **2f** and **2i** from series 2 being selected.

The results indicate a global decrease in the fluorescence emission in all cases, having recorded almost pure room temperature phosphorescence in all cases under these conditions, even in the presence of oxygen, in air-equilibrated solutions (see Fig. 4). The residual fluorescence emission in compound **1a** disappears after oxygen removal.

The phosphorescence quantum yields and lifetimes were also recorded achieving very interesting results with about 20–33% emission efficiency (Table 4). The large values of the emission lifetimes previously recorded under N_2-saturated conditions in solution are now achieved in air-equilibrated solid samples and increase to 400–925 μs when oxygen is removed, giving rise to emissive materials with quite interesting emission efficiencies and very long lifetimes, being half and one millisecond, respectively. This is mainly due to the reduction of the non-radiative deactivation pathways (restricted internal rotations around P–C bonds, among others) within the immobilized PMMA material (Table S4). These interesting photophysical properties would be relevant for the development of emissive materials with potential applications such as

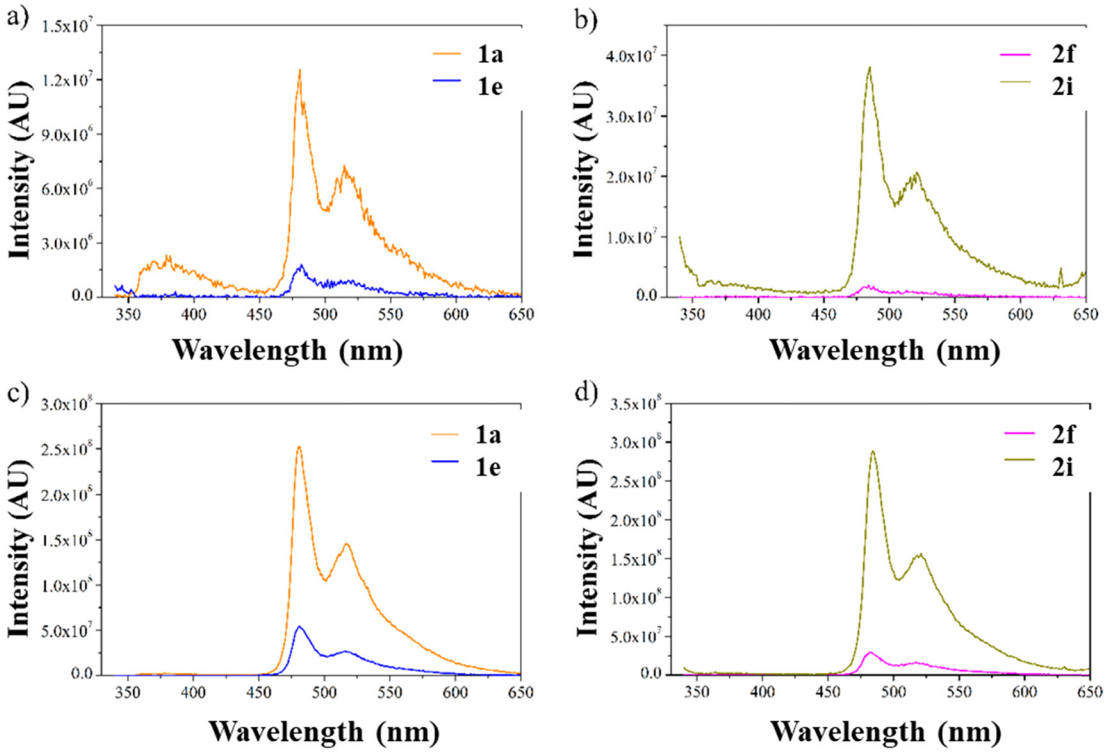

Fig. 4 Emission spectra of the selected compounds immobilized in PMMA matrixes under air equilibrated conditions (a) and (b) and nitrogen saturated samples (c) and (d).

Table 4 Emission quantum yields and lifetimes recorded for the compounds in PMMA

Compound	ϕ_{Ph} (air-eq.)	φ°_{Ph} (N_2-saturated)	τ_{Ph} (μs) (air-eq.)	τ°_{Ph} (μs) (N_2-saturated)
1a	0.03	0.25	137	926
1e	0.02	0.28	117	732
2f	0.02	0.20	62	427
2i	0.04	0.33	181	390

PhOLEDs,[42] Time-Gated Bioimaging & Sensing[43,44] and security and anti-counterfeiting.[45–48]

Conclusions

Gold(I) complexes incorporating a triphenylene chromophore and structurally diverse phosphane ligands have been successfully synthesized and analysed. Their photophysical response demonstrates a clear dependence on ligand steric and electronic properties, with dinuclear systems exhibiting increased phosphorescence contributions due to aurophilic interactions.

Immobilization in PMMA matrices efficiently suppresses non-radiative decay pathways, yielding materials with high phosphorescence quantum yields and extended lifetimes even under ambient conditions. These results showcase the promise of gold(I)-based systems as tunable, long-lived emissive materials suitable for technological applications in optoelectronics and luminescence sensing.

Experimental section

General procedures

All manipulations have been performed under prepurified N_2 using standard Schlenk-tube techniques. A solvent purification system (Innovative Technologies) was used to collect the solvents. 2-Ethynyltriphenylene (**L**)[31] and SPANphos[35] have been synthesized using described procedures. All other reagents were obtained from commercial suppliers and used as received.

Infrared spectra have been recorded on an FT-IR Nicolet™ iS™ 5 spectrophotometer. ^{1}H NMR (δ(TMS) = 0.0 ppm), ^{31}P{^{1}H} NMR (δ(85% H_3PO_4) = 0.0 ppm) and ^{13}C{^{1}H} NMR spectra were recorded at 400 or 500 MHz using Varian and Bruker spectrometers at 25 °C. ESI mass spectra have been recorded on a Fisons VG Quatro spectrometer. Absorption spectra have been recorded on a Varian Cary 100 Bio UV spectrophotometer, and emission spectra on a Horiba-Jobin-Ybon SPEX Nanolog spectrofluorimeter. Quantum yields have been recorded on a Hamamatsu Absolute PL Quantum Yield Spectrometer C11347. Luminescence lifetimes were measured on a JYF-DELTAPRO-NL equipment upon excitation of the samples with a 280 nm NanoLED and collecting the decays through a bandpass filter of 400 nm.

Single crystal data for compounds **1c** and **2i** were collected at BL13-XALOC beamline[49] of the ALBA synchrotron (λ = 0.72931) at 100 K. Crystals were mounted with Paratone N grease on a MiTegen kapton loop and placed in the N_2 stream of an Oxford Cryosystems Cryostream. Both structures were solved by intrinsic phasing (SHELXT)[50] and refined by full-matrix least squares

on F^2 using Olex2[51] utilising the SHELXL module.[52] Anisotropic displacement parameters were assigned to non-H atoms and isotropic displacement parameters for all H atoms were constrained to multiples of the equivalent displacement parameters of their parent atoms with U_{iso}(H) = 1.2$U_{eq.}$(CH) or 1.5$U_{eq.}$(CH_2, CH_3) of their respective parent atoms. CCDC 2481588 and 2482223 contain the supporting crystallographic data for the two structures.

Synthesis and characterization of gold(I) complexes

Synthesis of polymer [Au(L)]$_n$. Monoethynyltriphenylene (**L**) (57 mg, 0.23 mmol) in MeOH/THF (10 mL; v/v = 1 : 1) was reacted with sodium acetate (37 mg, 0.46 mmol) for 1 h at room temperature. Then, [AuCl(tht)] (72 mg, 0.22 mmol) was added, and a yellow precipitate was instantly generated. The mixture was stirred for 1 h at room temperature. Finally, the solid was filtered and dried under vacuum. IR ($\bar{\nu}$, cm^{-1}): 3079 (Csp^2-H st.), 1983 (C≡C st.) 1605 + 1488 (C=C st.), 748 (Csp^2-H be).

General synthesis for phosphane gold complexes

To a suspension of [Au(L)]$_n$ polymer (21 mg, 0.048 mmol) in 20 mL of CH_2Cl_2, a stochiometric amount of monophosphane (PMe_3, PEt_3, PPh_3, PTA, DAPTA) (0.048 mmol) or diphosphane (dppe, dppm, xantphos, spanphos) (0.024 mmol) was added, and the mixture was stirred for 1 hour. The solution was reduced to a small volume and hexane was added to precipitate the compound, that was filtered and dried under vacuum.

[Au(L)(PMe_3)] (1a). Yield: 71%. IR ($\bar{\nu}$, cm^{-1}): 3081 (Csp^2-H st.), 2966 (Csp^3-H st.), 2107 (C≡C st.), 1655 + 1487 (C=C st.), 753 (Csp^2-H be.). ^{1}H NMR (500 MHz, $CDCl_3$, 298 K): δ: 8.79 (d, ^4J = 1.6 Hz, 1H, H_1), 8.65–8.57 (m, 4H, H_4–H_7), 8.52 (d, ^3J = 8.6 Hz, 1H, H_3), 7.74 (dd, ^3J = 8.5 Hz, ^4J = 1.6 Hz, 1H, H_2), 7.69–7.57 (m, 4H, H_8–H_{11}), 1.62 (d, 9H, P-CH_3). ^{31}P{^{1}H} NMR (202 MHz, $CDCl_3$, 298 K): δ:1.2 (s). HR ESI-MS(+) m/z: 797.105 ([2M − L]$^+$, calcd 797.107); 547.088 ([M + Na]$^+$, calcd 547.087), 349.055 ([Au(PMe_3)$_2$]$^+$, calcd 349.055).

[Au(L)(PEt_3)] (1b). Yield: 68%. IR ($\bar{\nu}$, cm^{-1}): 3069 (Csp^2-H st.), 2966 + 2929 (Csp^3-H st.), 2116 (C≡C st.), 1605 + 1488 (C=C Ar st.), 1449 (CH_2 be.), 1379 (CH_3 be.), 759 (Csp^2-H be.). ^{1}H NMR (CD_2Cl_2, 400 MHz) δ: 8.70 (d, ^4J = 1.6 Hz, 1H, H_1), 8.67–8.60 (m, 4H, $H_{4–7}$), 8.53 (d, ^3J = 8.4 Hz, 1H, H_3), 7.68–7.64 (m, 5H, H_2,$_8$–H_{11}), 1.86 (dq, $^2J_{HP}$ = 9.6 Hz, $^3J_{HH}$ = 7.6 Hz, 6H, P-CH_2-CH_3), 1.24 (dt, $^3J_{HP}$ = 18 Hz, $^3J_{HH}$ = 7.6 Hz, 9H, P-CH_2-CH_3). ^{31}P{^{1}H} NMR (CD_2Cl_2, 161.9 MHz) δ: 38.3. ESI-MS(+) m/z: 567.15 ([M + H]$^+$, calcd 567.15), 589.14 ([M + Na]$^+$, calcd 589.13), 881.20 ([2M − L]$^+$, calcd 881.20), 1155.28 ([2M + Na]$^+$, calcd 1155.28).

[Au(L)(PPh_3)] (1c). Yield: 70%. IR ($\bar{\nu}$, cm^{-1}): 3051 (Csp^2-H st.), 2961 (C–H st.), 2112 (C≡C st.), 1604 + 1481 (C=C st.), 752 (Csp^2-H be.). ^{1}H NMR (400 MHz, $CDCl_3$, 298 K): δ: 8.84 (d, 1H, ^4J = 1.6 Hz, H_1), 8.66–8.58 (m, 4H, H_d), 8.54 (d, 1H, ^3J = 8.6 Hz, H_3), 7.79 (dd, 1H, ^3J = 8.5 Hz, ^4J = 1.6 Hz, H_2), 7.66–7.45 (m, 19H, PPh_3 + $H_{4–11}$). ^{31}P{^{1}H} NMR (161.9 MHz, $CDCl_3$, 298 K): δ: 42.3. HR ESI-MS(+) m/z: 1169.201 ([2M − L]$^+$, calcd 1169.201), 721.148 ([Au(PPh_3)$_2$]$^+$, calcd 721.149).

[Au(L)(PTA)] (1d). Yield: 92%. IR ($\bar{\nu}$, cm^{-1}): 2930 (Csp^3-H st.), 2116 (C≡C st.), 1603 + 1491 (C=C st.), 1451 (CH_2 be.), 757 (Csp^2-H be.). ^{1}H NMR (400 MHz, DMSO-d_6, 298 K) δ: 8.84–8.72 (m, 4H, $H_{4–7}$), 8.69 (d, ^3J = 8.7 Hz, 1H, H_3), 8.63 (d, ^4J = 1.4 Hz, 1H, H_1), 7.77–7.67 (m, 4H, $H_{8–11}$), 7.56 (dd, 1H, ^3J = 8.4Hz, ^4J = 1.5 Hz, H_2), 4.55 (d, ^2J = 12 Hz, 3H, P-CH_2-N), 4.38 (d, ^2J = 16 Hz, 3H, P-CH_2-N), 4.32 (s, 6H, N-CH_2-N). ^{31}P{^{1}H} NMR (161.9 MHz, DMSO-d_6, 298 K) δ: −48.6; HR ESI-MS(+) m/z: 606.134 ([M + H]$^+$, calcd 606.137), m/z: 511.12 ([Au(PTA)$_2$]$^+$, calcd 511.120), m/z: 158.084 ([PTA + H]$^+$, calcd 158.084).

[Au(L)(DAPTA)] (1e). Yield: 81%. IR ($\bar{\nu}$, cm^{-1}): 3051 (Csp^2-H st.), 2923 (Csp^3-H st.), 2109 (C≡C st.), 1637 (C=O st.), 1370 (CH_3 be.), 755 (Csp^2-H be. op.). ^{1}H NMR ($CDCl_3$, 400 MHz) δ: 8.79 (s, 1H, H_1), 8.64–8.57 (m, 4H, $H_{4–11}$), 8.54 (d, ^3J = 8.6 Hz, 1H, H_3), 7.73 (d, ^4J = 8.3 Hz, 1H, H_2), 7.67–7.62 (m, 4H, $H_{4–11}$), 5.78 (d, ^2J = 14.4 Hz, 1H, N-CH_2-N, H_b), 5.67 (d_{br}, ^2J = 15.9 Hz, ^3J = 7.2 Hz, 1H, P-CH_2-N, H_d), 4.93 (d, ^2J = 14.0 Hz, 1H, N-CH_2-N, H_c), 4.69 (d_{br}, 1H, P-CH_2-N, H_a), 4.63 (d, ^2J = 14.5 Hz, 1H, N-CH_2-N, H_c'), 4.18 (d_{br}, ^2J = 15.5 Hz, 1H, P-CH_2-N, Ha'), 4.05 (d, ^2J = 14.4 Hz, 1H, N-CH_2-N, H_b'), 3.9 (s, 2H, P-CH_2-N, H_e), 3.62 (dd, ^2J = 13.1 Hz, 1H, P-CH_2-N, H_d'), 2.11–2.10 (s + s, 6H, CH_3). ^{13}C{^{1}H} NMR ($CDCl_3$, 100 MHz) δ: 170.2 (C=O), 170.0 (C′=O), 130.9 (C_2), 130.1–129.4 (C_{4d}), 127.6–127.4 (C_1, C_4–C_{11}), 123.6–123.4 (C_3, C_4-C_{11}), 67.5 (N-CH_2-N, C_c), 62.3 (N-CH_2-N, C_b), 49.6 (d, J = 25.9 Hz, P-CH_2-N, C_e), 45.0 (d, J = 26.2 Hz, P-CH_2-N, C_a), 39.8 (d, J = 27.2 Hz, P-CH_2-N, C_d), 21.7 (CH_3), 21.4 (CH_3). ^{31}P{^{1}H} NMR ($CDCl_3$, 202 MHz) δ: −22.1. ESI-MS(+) m/z: 230.11 ([DAPTA + H]$^+$, calcd 230.11), 252.09 ([DAPTA + Na]$^+$, calcd 252.09).

[{Au(L)}$_2$(μ-dppe)] (2f). Yield: 86%. IR ($\bar{\nu}$, cm^{-1}): 3050 (Csp^2-H st.), 2947 (Csp^3-H st.), 2110 (C≡C st.) 1610 + 1487 (C=C st.), 1451 (CH_2 be.), 753 (Csp^2-H br). ^{1}H NMR (500 MHz, CD_2Cl_2, 298 K): δ: 8.76 (d, ^4J = 1.2 Hz, 2H, H_1), 8.60–8.68 (m, 8H, $H_{4–11}$), 8.56 (d, ^3J = 8.5 Hz, 2H, H_3), 7.74–7.85 (m, 8H, $H_{4–11}$), 7.72 (dd, ^3J = 8.5 Hz, ^4J = 1.5 Hz, 2H, H_2), 7.64–7.70 (m, 8H, PPh_2), 7.52–7.60 (m, 12H, PPh_2), 2.80 (s, 4H, PPh_2-CH_2-CH_2-PPh_2). ^{31}P{^{1}H} NMR (202 MHz, CD_2Cl_2, 298 K): δ: 39.4 (s). HR ESI-MS(+) m/z: 2612.469 ([2M + Na]$^+$, calcd 2612.474); 2337.387 ([2M − L]$^+$, calcd 2337.394); 1889.341 ([2M − AuL_2]$^+$, calcd 1889.342); 1441.285 ([2M − Au_2L_3]$^+$, calcd 1441.289); 1317.229 ([M + Na]$^+$, calcd 1317.230); 1043.152 ([M − L_1]$^+$, calcd 1043.155); 993.237 ([Au(dppe)$_2$]$^+$, calcd 993.237); 819.127 ([2M − AuL_3]$^{2+}$, calcd 819.128); 595.101 ([Au_2(dppe)$_2$]$^{2+}$, calcd 595.102).

Synthesis of [{Au(L)}$_2$(μ-dppm)] (2g). Yield: 93%. IR ($\bar{\nu}$, cm^{-1}): 3049 (Csp^2-H st.), 2957(Csp^3-H st.), 2105 (C≡C st.) 1607 + 148 (C=C st.), 1459 (CH_2 be.), 752 (Csp^2-H be.). ^{1}H NMR (400 MHz, CD_2Cl_2, 298 K) δ: 8.53 (d, ^4J = 1.1 Hz, 2H, H_1), 8.39 (d, 2H, ^3J = 8.0 Hz, H_3), 8.34–7.97 (m, 8H, $H_{4–11}$), 7.75–7.65 (m, 8H, $H_{4–11}$), 7.58 (dd, ^3J = 8.5 Hz, ^4J = 1.5 Hz, 2H, H_2), 7.55–7.27 (m, 20H, PPh_2), 3.71 (*t*, ^2J = 11.2 Hz, 2H, PPh_2-CH_2-PPh_2). ^{31}P{^{1}H} NMR (161.9 MHz, CD_2Cl_2, 298 K) δ: 32.4 (s). HR ESI-MS(+) m/z: 1303.214 ([M + Na]$^+$, calcd 1303.214), 1861.309 ([2M − AuL_2]$^+$, calcd 1861.309), 2309.362 ([2M − L]$^+$, calcd 2309.363), 2583.433 ([2M + Na]$^+$, calcd 2583.439).

Synthesis of [{Au(L)}$_2$({μ-xantphos})] (2h). Yield: 83%. IR ($\bar{\nu}$, cm^{-1}): 3066 (Csp^2-H st.), 2962 (Csp^3-H st.), 2107 (C≡C st.), 1604 + 1480 (C=C st.), 1258 (C-O st.), 752 (Csp^2-H be.). ^{1}H NMR (400 MHz, CD_2Cl_2, 298 K) δ: 8.73–8.51 (m, 10H, CH Ar), 7.70–6.60 (m, 38H, CH Ar), 1.70 (s, 6H, CH_3). ^{31}P{^{1}H} NMR

(161.9 MHz, CD_2Cl_2, 298 K) δ: 31.8. HR ESI-MS(+) m/z: 1223.209 ($[M - L]^+$, calcd 1223.211); 1353.351 ($[2M - Au_3L_4]^+$, calcd 1353.352); 1801.404 ($[2M - Au_2L_3]^+$, calcd 1801.404); 2249.449 ($[2M - AuL_2]^+$, calcd 2249.457).

[{Au(L)}$_2$(μ-spanphos)] (2i). Yield: 71%. IR ($\bar{\nu}$, cm^{-1}): 3047 (Csp^2-H st.), 2958 (Csp^3-H st.), 2109 (C≡C st.) 1606 + 1428 (C=C st.), 1364 (CH_3 be.), 1096 (C-O st.), 748 (Csp^2-H be.). ^{1}H NMR (500 MHz, CD_2Cl_2, 298 K) δ: 8.70–8.41 (m, 12 H, CH Ar), 7.93–7.16 (m, 32 H, CH Ar), 6.58 (dd, ^3J = 12 Hz, ^4J = 1.5 Hz, 2H, CH Ar, H_a), 2.06 (s, 6H, CH_3-Ph, H_b), 1.82 (d, ^2J = 14.5 Hz, 2H, R-CH_2-R, H_c), 1.70 (d, ^2J = 14.5 Hz, 2H, R-CH_2-R, H_c'), 1.2 (s, 6H, CH_3-R, H_d), 1.02 (s, 6H, CH_3-R, H_d'). ^{31}P{^{1}H} NMR (202 MHz, CD_2Cl_2, 298 K) δ: 34.9. HR ESI-MS(+) m/z: 1349.313 ($[M - L]^+$, calcd 1349.316), 901.263 ($[M - AuL_2]^+$, calcd 901.263).

Preparation with PMMA doped matrixes

The complex-doped film was prepared by drop-casting a mixture of the complex and the corresponding polymer onto a quartz substrate, as detailed below: to prepare the polymer solution, PMMA (molecular weight: 97 000) was dissolved in chloroform at a concentration of 200 mg mL^{-1}. Subsequently, 50 μL of polymer solution was added to the same volume a solution of the sample at a concentration of 2 mM. The films were drop cast onto a quartz substrate at room temperature to avoid any thermal annealing.

Conflicts of interest

There are no conflicts to declare.

Data availability

The data supporting the findings of this study, including synthetic procedures, spectroscopic data (NMR, IR, MS), photophysical measurements, and crystallographic information, are available within the article and its supplementary information (SI). Supplementary information is available. See DOI: **https://doi.org/10.1039/d5nj03389f**.

CCDC 2481588 (**1c**) and 2482223 (**2i**) contain the supplementary crystallographic data for this paper.[53a,b]

Acknowledgements

The authors are grateful to Project PID2022-139296NB-I00 funded by the Ministerio de Ciencia, Innovación y Universidades of Spain MCIU/AEI/10.13039/501100011033 and FEDER, UE and the Spanish network, Organometallic Chemistry for Sustainable Solutions − OASIS (RED2022-134074-T). This article is based upon work from COST Action CA22131, LUCES Supramolecular LUminescent Chemosensors for Environmental Security, supported by COST (European Cooperation in Science and Technology). A. A. also acknowledges IFARHU-SENACYT program in Panamá for the grant no. 270-2022-112 as PhD Scholarship. This research used the resources of the ALBA synchrotron. The corresponding crystallographic measurements were performed in collaboration with ALBA staff at the BL13-XALOC beamline.

References

1 V. R. Naina, S. Gillhuber, C. Ritschel, D. Jin, Shubham, S. Lebedkin, C. Feldmann, F. Weigend, M. M. Kappes and P. W. Roesky, *Angew. Chem., Int. Ed.*, 2024, **63**, e202414517, DOI: **10.1002/anie.202414517**.
2 A. Lazaro, M. Crespo, P. Pander, F. B. Dias and L. Rodriguez, *ACS Appl. Mater. Interfaces*, 2025, **17**, 31064–31077, DOI: **10.1021/acsami.4c22938**.
3 Y. Lu, X. Ma, X. Chang, Z. Liang, L. Lv, M. Shan, Q. Lu, Z. Wen, R. Gust and W. Liu, *Chem. Soc. Rev.*, 2022, **51**, 5518–5556, DOI: **10.1039/D1CS00933H**.
4 A. Casini and S. R. Thomas, *Chem. Lett.*, 2021, **50**, 1516–1522, DOI: **10.1246/cl.210238**.
5 R. P. Herrera and M. C. Gimeno, *Chem. Rev.*, 2021, **121**, 8311–8363, DOI: **10.1021/acs.chemrev.0c00930**.
6 J. C. Lima and L. Rodríguez, *Adv. Organomet. Chem.*, 2025, **83**, 139, DOI: **10.1016/bs.adomc.2025.04.002**.
7 M. I. Garcia, S. Burguera, A. Lazaro, A. Pinto, J. S. Ward, K. Rissanen, L. Rodriguez and A. Frontera, *Inorg. Chem.*, 2025, **64**, 10772–10779, DOI: **10.1021/acs.inorgchem.5c00372**.
8 Y. Zhou, W. Qin, C. Du, H. Gao, F. Zhu and G. Liang, *Angew. Chem., Int. Ed.*, 2019, **131**, 12230, DOI: **10.1002/anie.201906312**.
9 Q. Zheng, S. Borsley, G. S. Nichol, F. Duarte and S. L. Cockroft, *Angew. Chem., Int. Ed.*, 2019, **58**, 12617–12623, DOI: **10.1002/anie.201904207**.
10 A. Frontera and L. Rodríguez, *Adv. Inorg. Chem.*, 2024, **84**, 55–104, DOI: **10.1002/anie.201904207**.
11 H. Schmidbaur and H. G. Raubenheimer, *Angew. Chem., Int. Ed.*, 2020, **59**, 14748–14771, DOI: **10.1002/anie.201916255**.
12 R. A. Vogt, T. G. Gray and C. E. Crespo-Hernández, *J. Am. Chem. Soc.*, 2012, **134**, 14808–14817, DOI: **10.1021/ja303592q**.
13 E. Aguiló, A. J. Moro, M. Outis, J. Pina, D. Sarmento, J. S. Seixas de Melo, L. Rodríguez and J. C. Lima, *Inorg. Chem.*, 2018, **57**, 13423–13430, DOI: **10.1021/acs.inorgchem.8b01993**.
14 A. de Aquino, J. S. Ward, K. Rissanen, G. Aullón, J. C. Lima and L. Rodriguez, *Inorg. Chem.*, 2022, **61**, 20931–20941, DOI: **10.1021/acs.inorgchem.2c03351**.
15 L. Rodriguez, M. Ferrer, R. Crehuet, J. Anglada and J. C. Lima, *Inorg. Chem.*, 2012, **51**, 7636–7641, DOI: **10.1021/ic300609f**.
16 Y. Shen and J. J. Belbruno, *J. Phys. Chem. A*, 2005, **109**, 512, DOI: **10.1021/jp040502p**.
17 Y. Diack, S. Mallet-Ladeira, D. Lesage, J. V. S. Guerra, D. Bourissou and G. Szalóki, *Chem. Commun.*, 2025, **61**, 8003–8006, DOI: **10.1039/D5CC01540E**.
18 N. Svahn, A. J. Moro, C. Roma-Rodrigues, R. Puttreddy, K. Rissanen, P. V. Baptista, A. R. Fernandes, J. C. Lima and L. Rodríguez, *Chem. – Eur. J.*, 2018, **24**, 14654–14667, DOI: **10.1002/chem.201802547**.

19 H. Schmidbaur and B. A. Schier, *Chem. Soc. Rev.*, 2012, **41**, 370, DOI: 10.1039/C1CS15182G.
20 A. de Aquino, F. J. Caparros, K. N. Truong, K. Rissanen, M. Ferrer, Y. Jung, H. Choi, J. C. Lima and L. Rodriguez, *Dalton Trans.*, 2021, **50**, 3806–3815, DOI: 10.1039/d1dt00087j.
21 A. de Aquino, F. J. Caparros, G. Aullon, J. S. Ward, K. Rissanen, Y. Jung, H. Choi, J. C. Lima and L. Rodriguez, *Chem. – Eur. J.*, 2021, **27**, 1810–1820, DOI: 10.1002/chem.202004051.
22 P. Gründlinger, M. Gyorok, S. Wolfmayr, T. Breuer, D. Primetzhofer, B. Bruckner, U. Monkowius and T. Wagner, *Dalton Trans.*, 2019, **48**, 14712–14723, DOI: 10.1039/c9dt03049b.
23 M. D. N. Piña, S. Burguera, J. Buils, M. À. Crespi, J. E. Morales, J. Pons, A. Bauzá and A. Frontera, *ChemPhysChem*, 2022, **23**, e202200010, DOI: 10.1002/cphc.202200010.
24 A. Pinto, N. Svahn, J. C. Lima and L. Rodríguez, *Dalton Trans.*, 2017, **46**, 11125–11139, DOI: 10.1039/c7dt02349a.
25 C. R. Wade, A. A. Yakovenko and F. P. Gabbai, *New J. Chem.*, 2010, **34**, 1646–1651, DOI: 10.1039/C0NJ00128G.
26 J. J. Mihaly, A. T. Phillips, J. T. Malloy, Z. M. Marsh, M. Zeller, J. E. Haley, K. De La Harpe, T. A. Grusenmeyer and T. G. Gray, *Organometallics*, 2020, **39**, 489–494, DOI: 10.1021/acs.organomet.9b00768.
27 R. Gavara, E. Aguiló, J. Schur, J. Llorca, I. Ott and L. Rodríguez, *Inorg. Chim. Acta*, 2016, **446**, 189–197, DOI: 10.1016/j.ica.2016.03.012.
28 M. Ferrer, A. Gutierrez, L. Rodriguez, O. Rossell, J. C. Lima, M. Font-Bardia and X. Solans, *Eur. J. Inorg. Chem.*, 2008, 2899–2909, DOI: 10.1002/ejic.200800167.
29 J. J. Mihaly, S. M. Wolf, A. T. Phillips, S. Mam, Z. Yung, J. E. Haley, M. Zeller, K. De La Harpe, E. Holt, T. A. Grusenmeyer, S. Collins and T. G. Gray, *Inorg. Chem.*, 2022, **61**, 1228–1235, DOI: 10.1021/acs.inorgchem.1c02405.
30 A. de Aquino, N. Santamaria, A. J. Moro, D. Aguilà, A. Prieto, M. C. Nicasio, J. C. Lima and L. Rodriguez, *Inorg. Chem.*, 2025, **64**, 3392–3402, DOI: 10.1021/acs.inorgchem.4c04964.
31 A. P. Atencio, S. Burguera, G. Zhuchkov, A. de Aquino, J. S. Ward, K. Rissanen, J. C. Lima, I. Angurell, A. Frontera and L. Rodríguez, *Inorg. Chem. Front.*, 2025, **12**, 3041–3054, DOI: 10.1039/d4qi03225j.
32 R. B. Martínez, J. V. Alegre-Requena, R. P. Herrera and M. C. Gimeno, *Inorg. Chem.*, 2025, **64**, 17399–17408, DOI: 10.1021/acs.inorgchem.5c02714.
33 J. C. Lima and L. Rodríguez, *Chem. Soc. Rev.*, 2011, **40**, 5442–5456, DOI: 10.1039/c1cs15123a.
34 M. Pujadas and L. Rodríguez, *Coord. Chem. Rev.*, 2020, **408**, 213179, DOI: 10.1016/j.ccr.2020.213179.
35 Z. Freixa, M. S. Beentjes, G. D. Batema, C. B. Dieleman, G. P. F. van Strijdonck, J. N. H. Reek, P. C. J. Kamer, J. Fraanje, K. Goubitz and P. W. N. M. van Leeuwen, *Angew. Chem., Int. Ed.*, 2003, **42**, 1284–1287, DOI: 10.1002/anie.200390330.
36 C. Jiménez-Rodríguez, F. X. Roca, C. Bo, J. Benet-Buchholz, E. C. Escudero-Adán, Z. Freixa and P. W. N. M. van Leeuwen, *Dalton Trans.*, 2006, 268–278, DOI: 10.1039/B513870C.
37 C. Sobrerroca, I. Angurell, A. de Aquino, G. Romo, C. Jubert and L. Rodríguez, *ChemPlusChem*, 2023, **88**, e202300020, DOI: 10.1002/cplu.202300020.
38 F. Liu, G. Cao, Z. Feng, Z. Cheng, Y. Yan, Y. Xu, Y. Jiang, Y. Chang, Y. Lv and P. Lu, *ACS Appl. Mater. Interfaces*, 2023, **15**, 47307–47316, DOI: 10.1021/acsami.3c09433.
39 M. F. S. Khan, M. Akbar and J. Wu, *J. Fluoresc.*, 2025, **35**, 5239–5249, DOI: 10.1007/s10895-024-03905-4.
40 G. Romo-Islas, J. S. Ward, K. Rissanen and L. Rodriguez, *Inorg. Chem.*, 2023, **62**, 8101–8111, DOI: 10.1021/acs.inorgchem.3c00046.
41 A. Pinto, A. Llanos, R. M. Gomila, A. Frontera and L. Rodriguez, *Inorg. Chem.*, 2023, **62**, 7131–7140, DOI: 10.1021/acs.inorgchem.3c00197.
42 C. Wu, K. N. Tong, K. Shi, W. He, M. Huang, J. Yan, S. Li, Z. Jin, X. Wang, S. Jung, J. Ma, Y. Z. C. Yang, Y. Chi, R.-J. Xie, C. Yu, F. Kang and G. Wei, *Light: Sci. Appl.*, 2025, **14**, 156, DOI: 10.1038/s41377-025-01817-x.
43 B. Li, J. Lin, P. Huang and X. Chen, *Nanotheranostics*, 2022, **6**, 91–102, DOI: 10.7150/ntno.63124.
44 C. Liu, X. Wang, Y. Zhou and Y. Liu, *Sci. World J.*, 2013, **2013**, 801901, DOI: 10.1155/2013/801901.
45 H. Sun, S. Liu and W. Lin, *et al.*, *Nat. Commun.*, 2014, **5**, 3601, DOI: 10.1038/ncomms4601.
46 Y. Ma, K. Chen, J. Lu, J. Shen, C. Ma, S. Liu, Q. Zhao and W.-Y. Wong, *Inorg. Chem.*, 2021, **60**, 7510–7518, DOI: 10.1021/acs.inorgchem.1c00826.
47 S. Zhu, J. Hu, S. Zhai, Y. Wang, Z. Xu, R. Liu and H. Zhu, *Inorg. Chem. Front.*, 2020, **7**, 4677–4686, DOI: 10.1039/d0qi00735h.
48 W. Huang, X. Zhao, J. Zhang, L. Zhang, T. S. Cheung, Y. Xiao, F. Wang, Z. Zhao, S. Chen, L. Xu, Q. Shen and B. Z. Tang, *Adv. Funct. Mater.*, 2025, e12647, DOI: 10.1002/adfm.202312647.
49 J. Juanhuix, F. Gil-Ortiz, G. Cuní, C. Colldelram, J. Nicolás, J. Lidón, E. Boter, C. Ruget, S. Ferrer and J. Benach, *J. Synchrotron Radiat.*, 2014, **21**, 679–689.
50 G. M. Sheldrick, *Acta Crystallogr., Sect. A: Found. Adv.*, 2015, **71**, 3–8.
51 O. V. Dolomanov, L. J. Bourhis, R. J. Gildea, J. A. K. Howard and H. Puschmann, *J. Appl. Crystallogr.*, 2009, **42**, 339–341.
52 G. M. Sheldrick, *Acta Crystallogr., Sect. C: Struct. Chem.*, 2015, **71**, 3–8.
53 (*a*) CCDC 2481588: Experimental Crystal Structure Determination, 2025, DOI: 10.5517/ccdc.csd.cc2p997k; (*b*) CCDC 2482223: Experimental Crystal Structure Determination, 2025, DOI: 10.5517/ccdc.csd.cc2p9yqp.

